THE STUDY OF A DEBRIS CLOUD RISK ASSESSMENT IN GEOSYNCHRONOUS ORBIT

HARADA Ryusuke[(1)], KAWAMOTO Satomi[(1)], HANADA Toshiya[(2)]

[(1)] Japan Aerospace Exploration Agency (JAXA), 7-44-1 Jindaiji Higashi-machi, Chofu, Tokyo, 182-8522, Japan, kawamoto.satomi@jaxa.jp:
[(2)] Department of Aeronautics & Astronautics, Kyushu University, 744 Motooka, Nishi-ku, Fukuoka, 819-0395, Japan, hanada.toshiya.293@m.kyushu-u.ac.jp:

ABSTRACT

This paper reports the research on assessing the evolution and risk of an ejecta cloud generated in a geostationary orbit. In this orbit, collisions between intact objects and meteoroids/microdebris are expected to be dominant rather than objects larger than 10 cm. The small particles collisions scatter a large amount of secondary debris: ejecta into orbit, accumulating semi-permanently in the region. JAXA is now developing a probabilistic model to reveal the long-term behavior of this enormous amount of microdebris. This study conducts numerical simulations of ejecta cloud evolution using the probabilistic evolutionary model under development. The results are compared with JAXA's conventional evolutionary model, and their differences are discussed.

1 INTRODUCTION

Since the orbital period of objects in Geosynchronous orbit (GEO) synchronizes with the Earth's rotation, GEO objects can remain at a specified longitude above the equator, enabling such services as communications and broadcasting. According to the ESA's Annual Space Environment Report, the number of objects in GEO is increasing linearly since the launch of the first GEO satellite, Syncom 3, while the total mass and area of orbital objects in the region are increasing exponentially [1]. This behavior implies that the current satellites' structure is growing and becoming heavier with the demands of advanced missions and extension of operational duration. Moreover, there are some concepts for building the Space Solar Power System (SSPS) in GEO to achieve the sustainable use of clean energy [2]. SSPS is likely to be a massive structure with one side expected to be several kilometers in dimensions to generate plentiful electric power, which causes serious concerns to the debris environment. Due to a deficiency of atmospheric drag in the GEO region, the Post Mission Disposal (PMD) failed payloads, some old satellites launched before the Debris Mitigation Guidelines establishment, mission-related objects and new fragments stay in the region semi-permanently. Although the current spatial density in GEO is much lower than that of Low Earth Orbit (LEO), an increment in the number, area, and mass of GEO satellites would pose a higher collision probability and more resulting fragments in the future.

Since most GEO objects have an orbital inclination close to 0 degrees, the relative velocity of each object is less than 1–2 km/s, which is smaller than 10–15 km/s of LEO. By adopting the shielding design, McKnight implied that a collision with a debris particle smaller than 1 cm would not cause fatal damage to a payload [3]. However, the smaller the particle size, the greater the number, so objects' surface are degraded due to these collisions, and future mission may be interrupted if particles hit exposed cables or mission related components such as optical sensors. In the GEO region, collisions with outer meteoroids dominate in the particle size range of smaller than 1 cm. Some analysis with a debris environment model, MASTER-8, shows that meteoroids' collision velocities can be 5–25 km/s, sometimes up to 72 km/s [4]. The consequence of a collision in this speed range is under investigations due to the difficulty of ground-based Hyper Velocity Impact (HVI) tests and numerical simulations. However, the damage would be more severe. The evolution of the secondary microdebris ejecta produced in a Micrometeoroids and Orbital Debris (MMOD) collision is also important. Depending on the material, ejecta with masses dozens of times greater than that of the impacting object are generated. When MMOD hits a housing structure, the down-range ejecta mainly travels into the spacecraft interior, and the backscattered ejecta are emitted to outer space, while both ejecta are released to outer space when MMOD hits a thin structure such as a solar panel (see Fig. 1) [5]. Since the orbital fragments have a relatively high area-to-mass ratio, fragments decay eventually in atmospheric altitudes, whereas they will stay semi-permanently in higher altitudes. Ejecta emitted with low velocity will travel around a parental orbit, and those with high velocity will escape the parental orbit. Moreover, since the objects at the GEO altitude behave east-west libration, the periodical secondary collision risk between ejecta and a parent object should be considered. This longitudinal evolution can be changed by the breakup longitude [6]. The collision velocity between ejecta and other objects is considered to be smaller than that of meteoroid, however unlike meteoroid, ejecta accumulates in GEO, so the collision probability increases over the long term. In

Proc. 9th European Conference on Space Debris, Bonn, Germany, 1–4 April 2025, published by the ESA Space Debris Office
Editors: S. Lemmens, T. Flohrer & F. Schmitz, (http://conference.sdo.esoc.esa.int, April 2025)

order to evaluate the long-term evolution of an ejecta cloud and the secondary collision risk of the cloud in the GEO region, JAXA is studying the evolution of the orbital distribution and risk assessment of ejecta cloud generated by collisions with small particles, which are considered to be dominant in geostationary orbital environments.

This paper reports the latest research efforts to assess the evolution and risk of an ejecta cloud generated in GEO, and several computational simulations are conducted to reveal and discuss the behavior of a debris cloud in GEO using two debris environment evolutionary models: one is the Ejecta Cloud Analysis Tool (ECAT), and the other is the Near-Earth Orbital Debris Environment Evolutionary Model (NEODEEM).

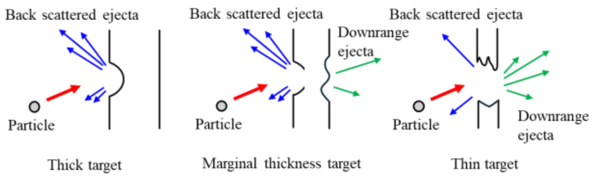

Figure. 1 Secondary debris: ejecta

2 GEO ENVIRONMENT

2.1 Cataloged Object Distribution

The US Space Surveillance Network (SSN) observes and maintains a catalog of Earth-orbiting objects. SSN catalogued objects are nominally larger than 10 cm in LEO and 1 m in GEO due to the difficulty of ground-based observations [7]. The Space Debris Mitigation Guidelines established by the Inter-Agency Space Debris Coordination Committee (IADC) define the GEO protection region as an altitude of 35,786 $\pm$ 200 km and an orbital inclination of $\pm$ 15° [8]. Table 1 lists catalogued objects in Space-track as of January 1, 2025, with apogee and perigee altitudes ranging from 35,586 to 35,986 km. Five of them incline more than 15°. The operational status and type of each object refer to the JAXA database. This database is annually updated based on the orbital situation as of January 1 of the year, which includes Space-track catalogued objects, objects observed by the JAXA telescope, and simulated fragments of past fragmentation events. The operational status of each object is judged based on the history of the Two Line Elements (TLE), whereas their type is based on literature surveys [9].

Table 1 Cataloged objects in GEO

Object Type	Number
Total	868
Operational	583
Non-operational	285
Drifting	189
Librating	96
Payload	780
Rocket Body	67
Mission Related Object	11
Others	10

The drift libration of non-operational objects is determined analytically, focusing on the J22 perturbation of the Earth's gravitational potential [10]. The specified energy of GEO objects E is represented by Eq. 1 using longitude λ and drift longitude $\dot{\lambda}$,

$$E = \dot{\lambda}^2 - 36{\Omega_\oplus}^2 J_{2,2}\left(\frac{\mathrm{R}_\oplus}{a_{GEO}}\right)^2 \sin^2(\lambda - \lambda_{2,2}) \qquad (1)$$

where the Earth's rotational speed is $\Omega_\oplus$, and the 2x2 general tesseral harmonics potential is $J_{2,2}$. The Earth's mean radius is $\mathrm{R}_\oplus$, and the GEO semimajor axis is a_{GEO}. The constants are summarized in Table 2. If E > 0, the GEO object exhibits drift and libration behavior when E < 0. The regime is energetically divided by a separatrix defined in Eq. 2.

$$\Delta a = \pm \frac{2a_{GEO}\Omega}{3\Omega_\oplus} \sin(\lambda - \lambda_{2,2}) \qquad (2)$$

Δa represents a relative distance from a_{GEO}, and Ω is a pendulum constant where $\Omega = 6\Omega_\oplus\sqrt{J_{2,2}}\frac{\mathrm{R}_\oplus}{a_{GEO}}$. Figs. 2 and 3 plot the drifting and librating objects in (Δa, λ) phase space and the longitudinal distribution of GEO cataloged objects, respectively. The longitudinal epoch is February 20, 2025. Most of the librating objects are trapped at a stable point at 75° east longitude (E75).

Table 2 Earth's geometrical and gravitational constant

Parameter	
$\Omega_\oplus$	6.300388 [rad/day]
$J_{2,2}$	1.815528 × 10^{-6}
$\lambda_{2,2}$	-0.260560204 [rad]
$\mathrm{R}_\oplus$	6378.14 [km]
a_{GEO}	42164.14 [km]

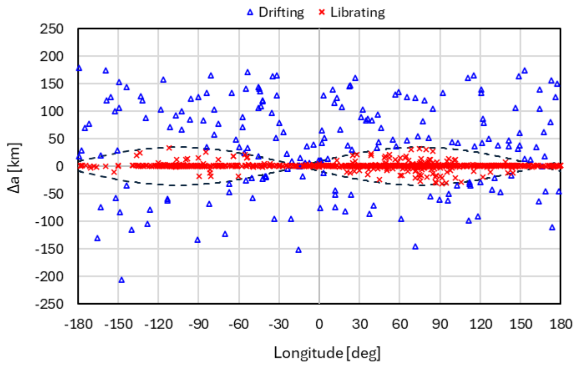

Figure. 2 Non-operational objects distribution in (Δa, λ) phase space

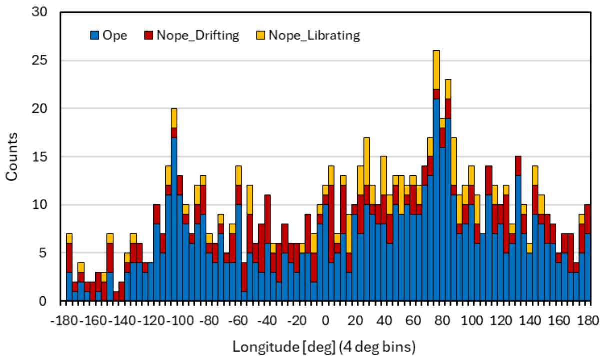

Figure. 3 Longitudinal distribution of GEO objects.

2.2 Small Debris Collision rate in GEO

Fig. 4-a plots an example of cumulative MMOD flux per size in GEO analyzed using orbital debris environment models MASTER-8 and ORDEM 3.2. The semimajor axis of the orbits of interest is 42,164.1 km, eccentricity is 1e-4, inclination is 0.01°, and analysis epoch is January 1 to December 31, 2025. Since the modelling approach of MASTER-8 and ORDEM is different, MASTER-8 flux in GEO below 1 cm diameter is ten to hundred times higher than that of ORDEM 3.2 while these models are similar at a high level. Furthermore, ORDEM 3.2 does not verify the flux below sub-10 cm in GEO. Therefore, this study used MASTER model. Fig. 4-b plots the relative MMOD flux of MASTER-8 normalized by total flux. In GEO, nearly 90% of the flux with particle size below 1 mm is meteoroid, and both meteoroid and manmade artifacts are present in the 1–10 cm range. Table 3 summarizes the expected collision rate of a normally sized satellite and SSPS for the MASTER-8 GEO flux shown in Fig. 4. The cross-sectional area is assumed to be 30 sq. m for a standard satellite and 4 sq. km for the SSPS. Even a standard satellite can collide with MMOD larger than 100 µm 100 times per year, and SSPS can experience tens of millions of collisions. More than 90% of these collisions are with meteoroids, whose collision velocity is several times faster than in LEO. The failure modes at meteoroid impact velocities have not been fully characterized because of the limitation of the particle ejection velocities in ground-based HVI tests. However, collisions with microdebris can severely damage spacecraft and produce many fragments [11], so the effects of meteoroid impact with extra-hypervelocity must be studied. The JAXA research and development directorate is conducting the co-research with University of Tokyo to develop a numerical simulator to predict ejecta dispersal behavior in extra-hypervelocity impacts [12].

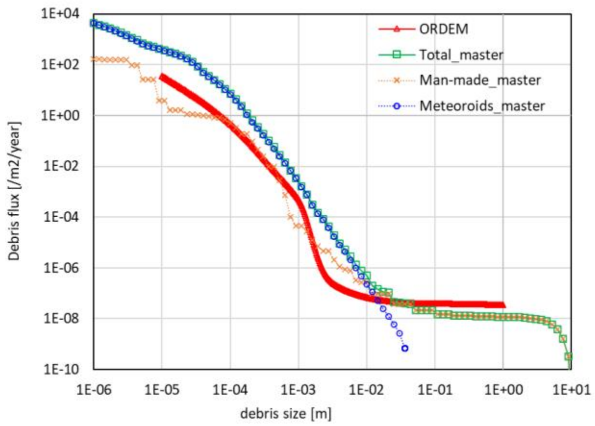

(a) MMOD flux in GEO with MASTER-8 and ORDEM 3.2. Total index of MASTER-8 is divided into Man-made and meteoroids.

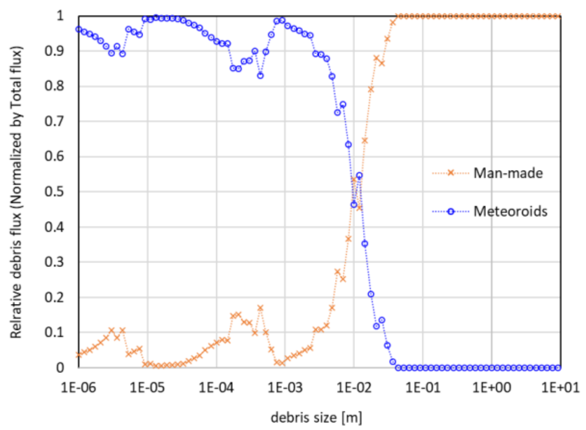

(b) Relative MMOD flux normalized by total flux (MASTER-8)

Fig. 4 Cumulative MMOD flux per size in GEO. The flux is determined by MASTER-8 and ORDEM 3.2, and the epoch is January 1 to December 31, 2025.

Table 3 Collision rate comparison calculated with MASTER flux

Particle size threshold	Collision rate [per year]	
	30 sq. m	4 sq. km
≥ 100 µm	Hundreds	Tens of millions
≥ 1 mm	~ 0.1	Thousands

≥ 1 cm	~1e-5	~10
≥ 10 cm	~1e-9	~1e-3

3 Numerical Simulation of GEO breakup

JAXA is developing an orbital evolution and risk assessment tool for ejecta clouds generated by meteoroid collisions that predominate in the GEO region in order to understand the long-term evolution and secondary collision risks of the cloud. This section summarizes the numerical simulation of a breakup in GEO using two orbital evolutionary models: the Ejecta Cloud Analysis Tool (ECAT), which is under development, and the Near-Earth Orbital Debris Environment Evolutionary Model (NEODEEM). The results are compared. This research simulates a self-breakup instead of particle collision since the ejecta model is still being developed. Table 4 shows the mass and orbital elements of the breakup object.

ECAT and NEODEEM apply the NASA Standard Breakup Model (NASA SBM) to simulate fragmentation [13]. The number of explosive fragments of size *Lc* or larger, in meters, is determined by Eq. 3,

$$N(L_c) = S6{L_c}^{-1.6} \quad (3)$$

where S is the scale factor. Approximately 310,000 explosive fragments larger than 1 mm are generated with a scale factor of 0.833 and injected into orbits. Fig. 5 plots the gabbard diagram of this breakup.

Table 4 Breakup object

Mass [kg]	SMA [km]	ECC	INC [deg]	λ [deg]
3500	42165.14	8.4e-5	0.04	135

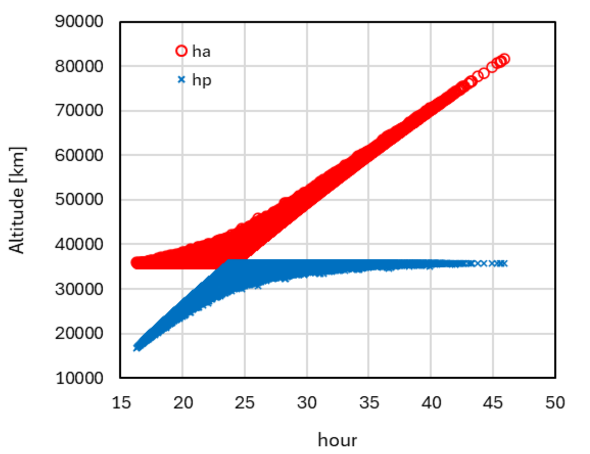

Figure. 5 Gabbard diagram of the simulated breakup.

3.1 Ejecta Cloud Analysis Tool

A collision with MMOD generates a large amount of ejecta, although it depends on the particle and target's material, impact velocity, and angle. Since some parts of the ejecta will travel around a parental orbit over the long term, and others will escape the parental orbit but periodically interfere with the parent object. Thus, the evolutional analysis of an ejecta cloud in GEO is important. A probabilistic model that assesses a debris cloud by converting particles to a continuum has an advantage in computational loads compared to a deterministic model, which calculates each object's evolution. Therefore, JAXA is now developing the ECAT probabilistic model to analyze ejecta cloud evolution in GEO. This model predicts the cloud evolution by converting a debris orbital distribution to a probability density distribution in an interest phase space and solving a continuity equation. This approach was developed for astronomy and is currently applied to predict the evolution of the LEO debris environment [14, 15]. The first to apply this method to the GEO debris cloud was Simone, which predicted a cloud density evolution analytically by approximating the drift-libration to a non-linear pendulum considering J22 perturbation [10]. This approach enables us to predict future distribution up to two years for orbit propagation error for debris within $a_{GEO} \pm 200$ km. As an early stage of ECAT development, this study reproduced Simone's method. Fig. 6 is the ECAT functional block diagram. ECAT predicts the debris cloud within $a_{GEO} \pm 200$ km for two years in $(\lambda, \dot{\lambda})$ phase space.

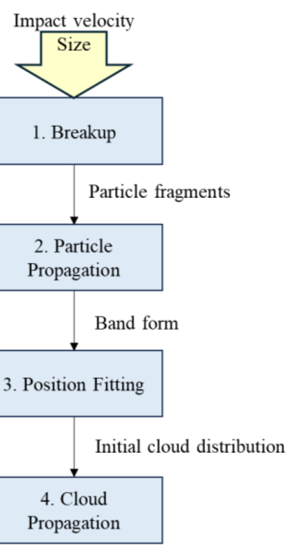

Fig. 6 Ejecta cloud analysis tool functional block diagram

A. Breakup

The model applied in this block is the NASA SBM. This study uses the explosion model since the ejecta distribution model is currently under development.

B. Particle Propagation

To consider the fragments as a cloud (probability density), it is necessary to orbitally propagate individual particles until the fragments diffuse to some extent. Evolutions of non-linear pendulum angles with J22 perturbation are described by Eqs. 4 and 5,

$$\begin{aligned} \theta(t) &= \mathrm{sgn}(\dot{\vartheta}_0) k\Omega[t - t_0] + \mathrm{sn}^{-1}(k_0|\kappa), \\ \lambda(t) &= \sin^{-1}\big(\mathrm{sn}(\theta(t)|\kappa)\big)\,\mathrm{sgn}(\mathrm{cn}(\theta(t)|\kappa)) + \lambda_{1,2}, \\ \dot{\lambda}(t) &= \tfrac{1}{2}\mathrm{sgn}(\dot{\vartheta}_0)\sqrt{\hat{E}_0}\,\mathrm{dn}(\theta(t)|\kappa). \end{aligned} \tag{4}$$

$$\begin{aligned} \Omega &= 6\Omega_{\oplus}\sqrt{J_{2,2}}\frac{\mathrm{R}_{\oplus}}{a_{GEO}}, \\ \hat{E}_0 &= \dot{\vartheta}_0{}^2 + E_p \sin^2\left({}^{\vartheta_0}/_2\right), \\ E_p &= 4\Omega^2, \\ k &= \sqrt{{}^{\hat{E}_0}/_{E_p}}, \\ \kappa &= {}^{1}/_{k}. \end{aligned} \tag{5}$$

where θ is the longitude relative to the vernal equinox and the subscript 0 represents the state quantity at the initial time. This study propagates each particle for two days with a time step of one day.

C. Position Fitting

After the particle propagation, fragments are converted to a probability density distribution in $(\lambda, \dot{\lambda})$ phase space. The converted cloud is the initial density n_0 of the cloud propagation. Two-Dimensional Probability Distribution Function (2D PDF) described in Eq. 6 is applied to position fitting.

$$\begin{aligned} n_0(\lambda, \dot{\lambda}) &= \frac{N_{frgm}}{2\pi\sigma_\lambda\sigma_{\dot{\lambda}}\sqrt{1-\rho^2}} \exp\left[-\frac{z}{2(1-\rho^2)}\right], \\ z &\equiv \frac{(\lambda-\mu_\lambda)^2}{\sigma_\lambda{}^2} - \frac{2\rho(\lambda-\mu_\lambda)(\dot{\lambda}-\mu_{\dot{\lambda}})}{\sigma_\lambda\sigma_{\dot{\lambda}}} + \frac{(\dot{\lambda}-\mu_{\dot{\lambda}})^2}{\sigma_{\dot{\lambda}}{}^2}, \\ \rho &\equiv \mathrm{cor}(\lambda, \dot{\lambda}) = \frac{V_{\sigma_\lambda\sigma_{\dot{\lambda}}}}{\sigma_\lambda\sigma_{\dot{\lambda}}}, \end{aligned} \tag{6}$$

where ρ is the correlation of λ and $\dot{\lambda}$, $V_{\sigma_\lambda\sigma_{\dot{\lambda}}}$ is the covariance, and σ_λ and $\sigma_{\dot{\lambda}}$ are the variance of the fragment's longitudes and drift longitudes. $(\lambda, \dot{\lambda})$ phase space is divided by $\lambda \times \dot{\lambda}$: 1000 × 300.

D. Cloud Propagation

Since this study does not consider source-tank terms corresponding to new launches, natural decay, or PMD activities, the continuum equation can be expressed by Eq. 7.

$$\begin{aligned} &\frac{\partial n}{\partial t} + v_\lambda \frac{\partial n}{\partial \lambda} + v_{\dot{\lambda}} \frac{\partial n}{\partial \dot{\lambda}} = -n\left[\frac{\partial v_\lambda}{\partial \lambda} + \frac{\partial v_{\dot{\lambda}}}{\partial \dot{\lambda}}\right], \\ &v_\lambda = \frac{d\lambda}{dt} = \dot{\lambda}, \\ &v_{\dot{\lambda}} = \frac{d\dot{\lambda}}{dt} = 18\Omega_{\oplus}{}^2 J_{2,2}\left(\frac{\mathrm{R}_{\oplus}}{a_{GEO}}\right)^2 \sin 2(\lambda - \lambda_{2,2}). \end{aligned} \tag{7}$$

By applying the method of characteristics, the probability density at a specific time is given by Eq. 8.

$$n(\lambda, \dot{\lambda}, t) = n_0\left(\tilde{\lambda}, \tilde{\dot{\lambda}}, t\right) \tag{8}$$

$\tilde{\lambda}, \tilde{\dot{\lambda}}$ are obtained by inverting the characteristic at the initial time. A backward propagation in time is performed using Eq. 9 to retrieve these elements since the analytical solution cannot be derived [10]. This study propagates a cloud for two years in five-day steps.

$$\begin{aligned} \theta(t) &= \mathrm{sgn}(\dot{\vartheta}_0) k\Omega[t - t_0] + \mathrm{sn}^{-1}(k_0|\kappa), \\ \tilde{\lambda}(t) &= \sin^{-1}\big(\mathrm{sn}(\theta(t)|\kappa)\big)\,\mathrm{sgn}(\mathrm{cn}(\theta(t)|\kappa)) + \lambda_{1,2}, \\ \tilde{\dot{\lambda}}(t) &= \tfrac{1}{2}\mathrm{sgn}(\dot{\vartheta}_0)\sqrt{\hat{E}_0}\,\mathrm{dn}(\theta(t)|\kappa). \end{aligned} \tag{9}$$

The evolution of fragments within $a_{GEO} \pm 200$ km generated from the breakup object in Table 4 is analyzed for two years by ECAT. Since the 2D PDF is almost independent of the specific run of the NASA SBM [10], this study simulates one Breakup segmentation run. The grid distances in phase space are set to $\Delta\lambda \equiv 0.36$ deg and $\Delta\dot{\lambda} \equiv$ 1.98e-7 deg/s according to the fragments' maximum and minimum drift longitude $\pm$ 2.97e-7 deg/s.

Fig. 7 shows the debris cloud evolution for two years. After fragmentation, the cloud at the breakup longitude spreads into the overall phase space. Librating fragments are trapped at the nearest gravity potential well (E75) and are expected to interfere with the parent object within several years. At this breakup longitude, the cloud does not go beyond the gravity potential and is not trapped at the next gravity well (W105). Therefore, the libration will not occur in the western well for two years. The drifting fragments are distributed either eastward or westward and pass near the parent object. The cumulative collision probability with a particular target satellite evaluates the risk of secondary collisions with debris clouds with these different behaviors.

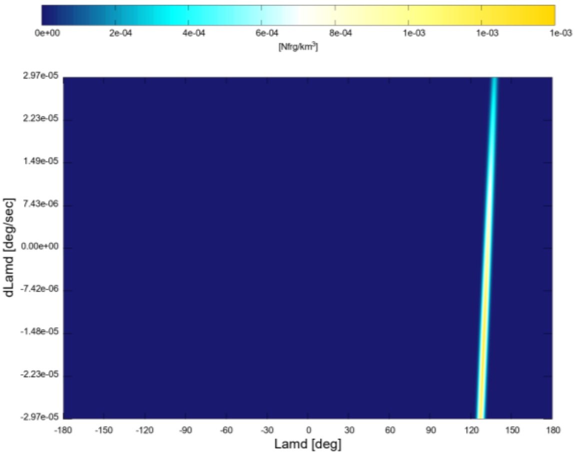

(a) Debris cloud density distribution after two days

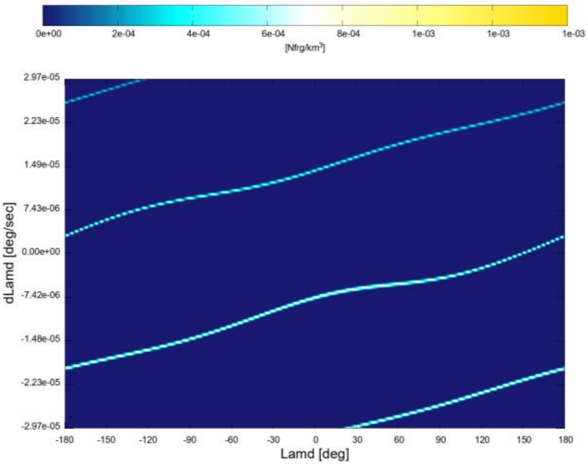

(b) Debris cloud density distribution after six months

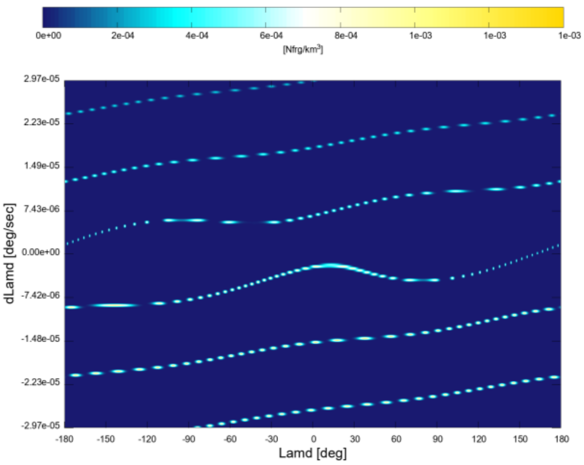

(c) Debris cloud density distribution after one year

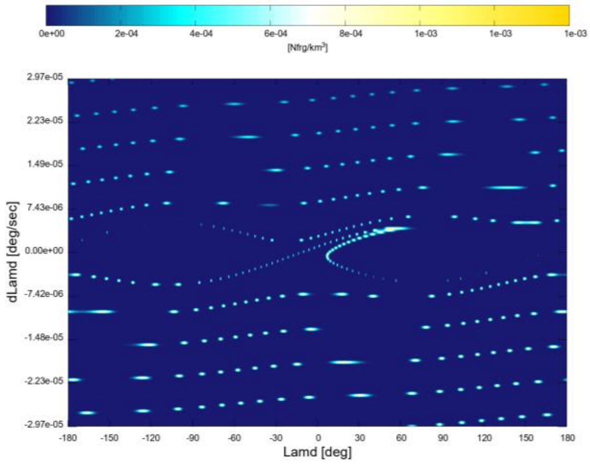

(d) Debris cloud density distribution after two years

Fig. 7 Debris cloud density evolution in $(\lambda, \dot{\lambda})$ phase space over two years. The parent object broke up at 135 degrees east longitude.

Based on the kinetic theory of gases, the target's cumulative collision probability crossing a debris cloud can be calculated from the mean collision rate N in each interval of time T. This can be written as Eq. 10:

$$N = \rho v_{rel} A_c T \tag{10}$$

where ρ is the spatial density, v_{rel} is the relative velocity, and A_c is the cross-sectional area, where the root of the square sum of the particle and target area is $A_c = \sqrt{A_p^2 + A_t^2}$. The relative velocity is a function of the GEO orbital velocity and the relative inclination between the projectile and target. This study assumed 536 m/s at the average inclination distribution of 10° in GEO [16]. Normally sized satellite and SSPS are considered targets, with cross-sectional areas of 30 sq. m and 4 sq. km, respectively. The average area of fragments is 0.99 sq. m.

Fig. 8 shows the distribution of cumulative collision probability for two years. Corresponding to the evolution of the density distribution, most debris is trapped in gravity well E75, resulting in a high cumulative collision probability. Since the velocity of the debris cloud was not considered, and impact velocity was assumed to be constant, the collision probability was equal in the area where the breakup longitude and the librating cloud passed through. However, the collision probability would change at stable and unstable points. Furthermore, the interval time is set to the time step of backward propagation for five days, but fragments with a significant drift rate are moved to another longitude grid during this time. Therefore, some of the drifting objects were overestimated. The two-year cumulative collision probability at 135° east longitude (E135) is 1.87e-4 for the normally sized satellite and 24.96 for SSPS.

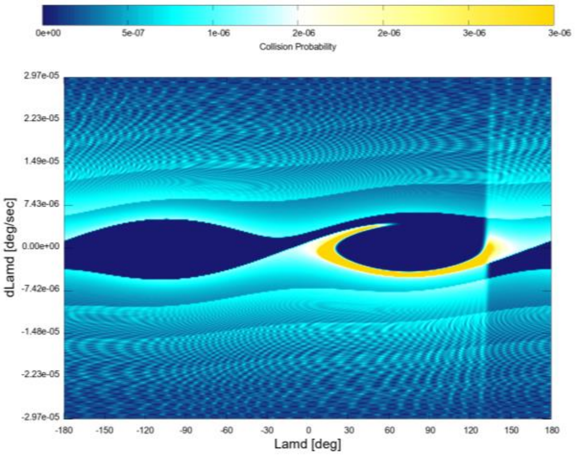

(a) Target: normally sized satellite (A_t = 30 sq. m)

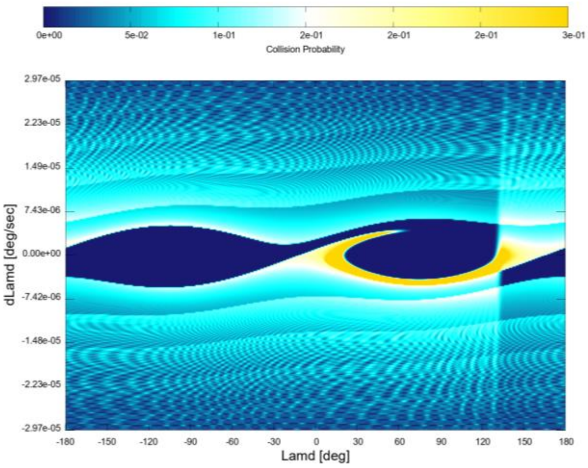

(b) Target: SSPS (A_t = 4 sq. km)

Figure. 8 Cumulative collision probability to target satellite for 2 years

3.2 Near-Earth Orbital Debris Environment Evolutionary Model

NEODEEM is a deterministic model developed by Kyushu University and JAXA that calculates orbital propagations and fragmentation simulations of each orbital object [17]. NEODEEM conducts the long-term orbital propagation of six Keplerian elements considering the Earth's 4×4 gravitational potential, solar radiation pressure, the third body's attraction, and atmospheric drag. Fragmentation events are simulated using a random number generator, and new fragments are generated according to the NASA SBM. The mean value of 100 Monte Carlo (MC) simulations is shown. This subsection simulates the long-term evolution of the same fragmentation in Subsection 3.1 using NEODEEM. A hundred runs of NASA SBM are conducted to generate fragments from the parent object in Table 4, and the fragments are deployed into orbits as an initial population for each MC. This scenario does not consider other background objects, such as existing GEO objects. No new launch activities, collision events, or explosions are assumed. The analysis epoch is from January 1, 2024, to January 1, 2124.

Fig. 9 plots the evolution of the effective number (EN) of objects. The figure on the top shows EN in each altitude band and the one at the bottom shows EN crossing at the altitude of $a_{GEO} \pm 200$ km, of which the inclination magnitude exceeds 15 degrees. Most of the fragments distributed within the altitude of $a_{GEO} \pm 200$ km. The 53-year periodic orbital inclination oscillations due to the third object attraction cause debris in the GEO protection region to pass through from out of the plane with a larger inclination angle. Although the period of inclinational oscillation changes because the mean altitude of each debris varies due to the evolution of eccentricity caused by perturbations, some parts of the fragments show the out-of-plane behavior again around 2105. The total amount of debris passing through the GEO protection region does not change much after 100 years.

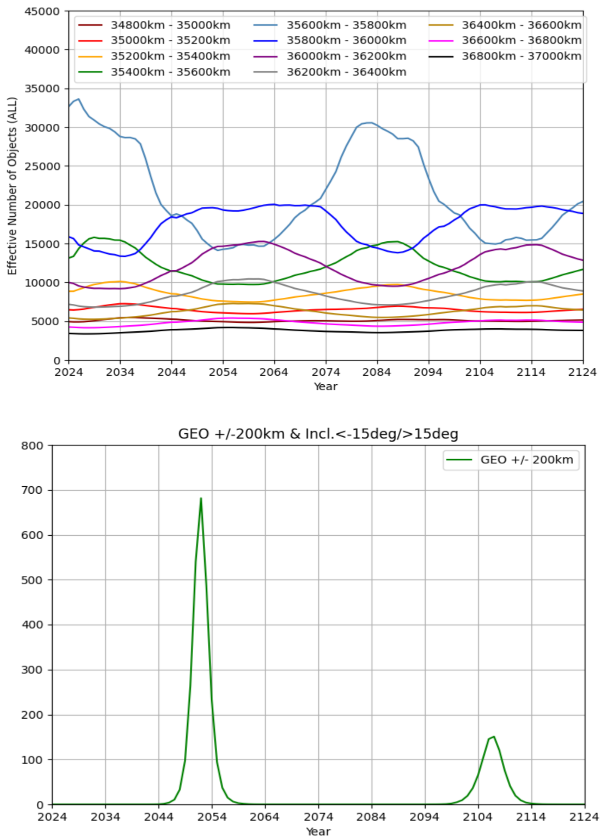

Figure. 9 Evolution of the effective number (EN) of fragments. The figure on the top shows EN in each altitude band, and the one at the bottom shows EN crossing at the altitude of $a_{GEO} \pm 200$ km, of which inclination is larger than ±15 degrees.

NEODEEM calculates the collision probability between individual objects: C_{12} by Eq. 11,

$$C_{12}=\frac{p_2\Delta V}{V}\frac{p_1}{V}A_{12}U_{12},$$
$$A_{12}=\pi(d_1+d_2)^2/4 \tag{11}$$

where V is the volume of each error sphere, ΔV is the overlapping volume of two error spheres, p_1 and p_2 are the probabilities of objects existing within the error spheres, A_{12} is the effective collision area, and U_{12} is the relative velocity, respectively. Target satellites: a normally sized satellite and SSPS are placed at E135 to assess the collision probability of the debris cloud. The cross-sectional areas of the targets are the same as described in Subsection 3.1. The targets are operational for the first 20 years, maintaining their altitudes and eccentricities. Details of the targets are summarized in Table 5, which shows the cumulative collision probability (i.e., the expected number of collisions between a target and the debris) cloud for 100 years.

Table 5 Target satellites details

Parameter	
Mass	3,500 kg (normal) 20,000 ton (SSPS)
Cross-sectional Area	35 sq. m (normal) 4 sq. km (SSPS)
SMA [km]	42167.14
ECC	9.34e-5
INC [deg]	0.036
RAAN [deg]	320.07
AoP [deg]	194.04
MA [deg]	75.8

Fig. 10 shows the expected number of collisions (ENc) between a target and the debris cloud for 100 years. ENc increases in both cases in the long term. The slope becomes slightly higher after 2044 since the target's end operation and its orbits change. The periodic increase in ENc indicates the interference with librating fragments. The ENc of the normally sized satellite with fragments larger than 1 mm is 2.2e-5 after two years and 5.5e-4 after 100 years; for SSPS, it is 2.35 after two years and 75 after 100 years. Compared with the ECAT, NEODEEM results are one-tenth as large as that of ECAT because ECAT does not consider the altitudinal evolution of a cloud, and ENs with all the initial fragments in the GEO region are considered.

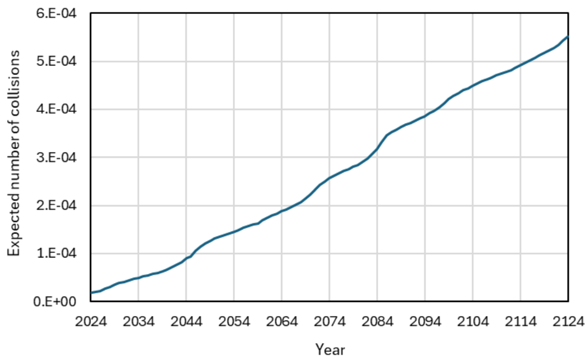

(a) Target: normally sized satellite (A_t = 30 sq. m)

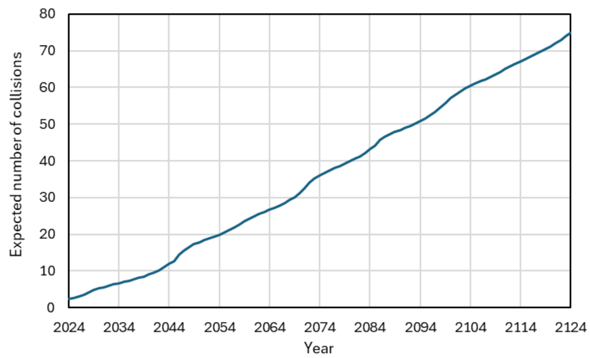

(b) Target: SSPS (A_t = 4 sq. km)

Figure. 10 Expected number of collisions between the debris cloud and target satellite for 100 years

4 Future Development

The following two functions are being investigated to assess the accumulation and secondary risks of an ejecta cloud generated by a collision between a GEO object and MMOD.

Ejecta Cloud Generation

ECAT implements the NASA SBM in the breakup scenario. While this model is appropriate to simulate a self-breakup, which rarely occurs in GEO, it is unsuitable for ejecta generation, such as fragment direction and velocity distribution due to meteoroid collisions, which are believed to predominate in GEO. Therefore, the implementation of the ejecta generation model ONERA synthesis model [18] is considered. Onera developed this model in collaboration with ESA based on a synthesis of available experimental data and theoretical/numerical results on ejecta. It provides mass, size, and number of particles, considering the probability density distribution in the zenith-azimuth angle. The ejecta distribution by ONERA is relative to a target's body face, which requires converting the coordinate system to the inertial frame for an orbital evolutionary calculation.

Cloud Propagator

Since ECAT considers the J22 perturbation only, this model provides the analytical evolution of an ejecta cloud in GEO for two years. However, it is unsuitable for assessing ejecta accumulation's long-term effect due to the limited dynamics model and calculation period. ECAT uniformly converts fragments at a_{GEO} ±200 km to (λ, $\dot{\lambda}$) phase space and does not consider the altitude distribution, resulting in an overestimate of collision probability with the target satellites. The assumption of drift-libration in GEO to the non-linear pendulum is effective for short-term evolution, however longitudinal errors cannot be ignored for long-term assessment. Furthermore, the collision velocity is constant because ECAT does not consider the orbital evolutions of fragments. Based on the above, ECAT orbit propagators are considered to extend the phase space to (a, e, i, λ) phase space and implement third-object attraction and solar radiation pressure.

5 Conclusion

This paper reported the latest research efforts to assess the evolution and risk of an ejecta cloud generated in a geostationary orbit, and several computational simulations were conducted to reveal and discuss the behavior of a debris cloud in GEO using two debris environment evolutionary models: ECAT which are under development, and NEODEEM which is a conventional model developed with Kyushu University.

ECAT analysis showed the short-term evolution of an ejecta cloud in (λ, $\dot{\lambda}$) phase space that the cloud gathers at the breakup longitude after fragmentation spreads to the overall phase space. Librating fragments were trapped at the nearest gravity potential well and expected to interfere with the parent object several years later. The drifting fragments were distributed either eastward or westward and passed in the parent object's vicinity. NEODEEM analysis showed the long-term evolution of the GEO fragments in six Keplerian elements. The 53-year periodic orbital inclination oscillations due to the third body attraction caused debris in the GEO protection region to pass through from out of the plane with a larger inclination. The total amount of debris passing through the GEO protection region will not change much after 100 years. The cumulative collision probability of target satellites calculated by ECAT and NEODEEM were compared. ECAT results were ten times larger than that of NEODEEM because ECAT calculates only the longitudinal evolution of a cloud considering J22 perturbation, and ENs with all the initial fragments in the GEO region were converted to the probability density.

This paper introduces two future development plans: implementing the ejecta cloud generator and improving the cloud propagator to assess the long-term effects of an ejecta cloud.

Acknowledgments

We used JAXA Supercomputer System Generation 3 (JSS3).

Reference

1. ESA Space Debris Office, ESA's Annual Space Environment Report, Issue/revision 8.0, July 19, 2024, pp 24-25.
2. Sasaki, S., Tanaka, K. et al., A new concept of solar power satellite: Tethered-SPS, Acta Astronautica **60** (2006) 153-165.
3. Darren S. McKnight, Frank R. Di Pentino, New insights on the orbital debris collision hazard at GEO, Acta Astronautica **85** (2013) 73–82.
4. Satomi Kawamoto, Nobuaki Nagaoka, Ryusuke Harada, Toshifumi Yanagisawa, Yugo Kimoto, and Daisuke Joudoi, Debris Sweepers in High Orbit - Debris Bumpers That Do Not Generate Ejecta, 73rd International Astronautical Congress (IAC), Paris, France, 18-22 September 2022.
5. IADC Working Group 3, CHARACTERIZATION OF EJECTA FROM HVI ON SPACECRAFT OUTER SURFACES, IADC-11-05, Revision 1, April 2013.
6. Paul V. Anderson, Hanspeter Schaub, Longitude-dependent effects of fragmentation events in the geosynchronous orbit regime, Acta Astronautica **105** (2014) 285–297.
7. Space-track.org, https://www.space-track.org/#ssr (accessed January 24, 2025)
8. IADC Steering Group and Working Group 4, IADC Space Debris Mitigation Guidelines, IADC-02-01, Revision 2, March 2020.
9. UEDA O. Hiroko, HIROIKE Naruya, NAGAOKA Nobuaki, HATTA Shinji, KOBAYASHI Taizo, KAWAMOTO Satomi, HARADA Ryusuke, NITTA Kumi, Development of Tools and Database for Space Debris Mitigation, 11th JAXA Space Debris Workshop, Tokyo, Japan, 28-30 October 2024.
10. Piani Simone, "Analytical Model for Propagation of Debris Clouds in Geostationary orbit", 2022, Politecnico di Milano, Faculty of Industrial Engineering, Master in Space Engineering, Supervisor: Camilla Colombo, Co-supervisor: Andrea Muciaccia, Printed in Italy.
11. Hajime Yano, Design and Verification of Deep Spacecraft Shields Against Extreme Hypervelocity Impacts: A review, 11th JAXA Space Debris Workshop, Tokyo, Japan, 28-30 October 2024.
12. Sho Kajihara, Souichi Maruyama, et al., Numerical analysis modeling for quantitative prediction of ejecta dispersal behavior due to hyper-velocity impact, 9th European Conference on Space Debris, Bonn, Germany, 1-4 April 2025. (Submitted)
13. J.-C., Liou, N., Johnson, P., Krisko, and P., Anz-

Meador. The new NASA orbital debris breakup model NASA breakup model, Proc. pf the IAU Colloquium **181**, Volume 15, 2002, pp.363-36.

14. Francesca Letizia, Camilla Colombo, Hugh G. Lewis, Multidimensional extension of the continuity equation method for debris clouds evolution, Advances in Space Research **57** (2016) 1624–1640.
15. Frey, S. (2020), Evolution and hazard analysis of orbital fragmentation continua, Doctoral thesis, Politecnico di Milano, Supervisors: Colombo, C., Lemmens, S. and Krag., H.
16. Darren S. McKnight n, Frank R. Di Pentino, New insights on the orbital debris collision hazard at GEO, Acta Astronautica **85** (2013) 73–82.
17. Ryusuke Harada, Satomi Kawamoto, Toshiya Hanada, Assessments of the impacts of orbital fragmentations using the Near-Earth Orbital Debris Environment Evolutionary Model (NEODEEM), Journal of Space Safety Engineering Volume **11**, Issue 3, September 2024, Pages 395-402.
18. IADC Working Group 3, Characterization of Ejecta from HVI on Spacecraft Outer Surfaces, IADC-11-05, Revision 1, June 2012.